APEM journal ISSN 1854-6250 *Advances in Production Engineering & Management* 5 (2010) 1, 33 - 44 Scientific paper

WORKABILITY STUDIES ON Al-20%SiC POWDER METALLURGY COMPOSITE DURING COLD UPSETTING

Ramesh,T. *; Prabhakar, M* & Narayanasamy, R**
* Department of Mechanical Engineering, National Institute of Technology, Tiruchirappalli, India.
** Department of Production Engineering, National Institute of Technology, Tiruchirappalli, India.
E-mail: tramesh@nitt.edu, mprabha2000@rediffmail.com

Abstract:
The application fields of bulk metals have been limited because of their lack of workability criteria. Powder metallurgy composites have superior mechanical properties such as high strength, elastic strain limit and fracture toughness and workability behaviour. In order to improve the workability criteria, conducting experiments under cold conditions so as to investigate the super plastic behaviour of the materials, has been investigated during cold upsetting. The present study has been performed to evaluate the effect of the workability behaviour of pure Aluminium and Al -20% SiC powder metallurgy composites introducing various sizes of the second phase particles, namely, 120 μm, 65 μm and 50 μm and for the aspect ratios of 0.9 and 1.2. The effect of second phase particle size on the workability of the material composites proposed has been investigated over this work. The experimental results were analyzed under triaxial stress state condition. The formability stress index, various stress ratio parameters were obtained for each particle size additions and aspect ratios. The relationship between various stresses against the axial strain has been studied.

Key Words: Metal Matrix Composite, Aluminium, Silicon Carbide, Plastic Behaviour

1. INTRODUCTION

Metal forming is an important plasticity working technique, which is used in many types of applications especially in the industrial products of light weight and high strength. Many authors have found that the composite materials are stronger than conventional alloys [1, 2]. Particle reinforced Aluminium alloy matrix composite is one of the best material to replace the conventional structural alloys. However, the demand for such materials has been limited to high cost applications due to their complex processing. Powder metallurgical technique is one the most excellent route of low cost processing to produce high quality products of near net shape.

The ductile failure of the Al matrix has been studied for the nucleation, growth and coalescence of voids [3]. Studies have revealed that the Al-SIC composite gives better tensile fatigue performance compared to monolithic alloy [4]. Compression deformation test on Al-5%SiC composite has been carried out at elevated temperature and it has been found that the SiC added Al P/M composite gives better formability compared to pure Al and proved thro FEM technique [5].

Workability is concerned with the extent to which a material can be deformed in a specific metal working process without the initiation of cracks [6]. The cold forging process has major limitation on crack formation. So the ductile fracture prediction is very important for the cold forging operations. The prediction of ductile fracture in metalworking operations has therefore attracted the attention of many researchers for more than five decades. The prediction of powder metallurgical composite's fracture initiation increases the composite usages in a safe environment without failure. This will be useful to produce near net shape products to improve the quality of P/M products.

Shima and Oyane [7] studied the frictionless closed-die compression. The stresses in the direction of compression have been evaluated in relation to the relative density. A new yield function for compressible powder metallurgy materials was proposed by Doraivelu et al. [8]. The yield function has been derived based upon a yield criterion and this function was experimentally verified for the uniaxial state of compressive stress using the P/M Aluminium alloy. But this function has not been verified with other state of stresses.

Workability criterion of P/M compacts have been discussed by Abdel-Rahman et al., [9], investigating the effect of relative density on the forming limit of P/M compacts during upsetting. These authors also have proposed the criteria called formability stress index (β) for describing the effect of the mean stress and the effective stress with the help of two theories, proposed by Kuhn-Downey and Whang-Kobayashi. Further, authors have extended their investigations on the effect of relative density on the formability stress index (β) and concluded that the workability has quantitative relationship with the density. The effect of relative density can be measured by the simple experiments.

A new generalized yield criterion of porous sintered P/M metals was proposed by Narayanasamy and Ponalagusamy [10], considering an anisotropic parameter. In addition, a new flow rule with anisotropic parameter for porous metal was also proposed. Satsangi et al. [11] studied the forging behaviour and densification of porous powder metal both theoretically and experimentally. They presented incremental and piecewise linear elastic plastic finite element method for analysis of forging. Narayanasamy et al. [12] presented some of the important criteria generally used for the prediction of workability.

In this paper, a complete investigation on the workability criteria of Al and Al-20% SiC powder preforms was made during cold upsetting. Powder metallurgy preforms with various particle size and aspect ratios were discussed for studying the behaviour of workability during cold upsetting under triaxial stress state condition.

2. EXPERIMENTAL DETAILS

2.1 Compacts preparation

Atomized Aluminium powder of -100 μm was procured and analyzed for its purity. The same was found to be 99.7 percent and 0.3% insoluble impurities. The characterization of Al powder was studied by determining the flow rate, apparent density and particle size distribution and the details are listed in Table I. To investigate the particle size distribution, Metallographic studies were made with Scanning Electron Microscope and the image is provided in Figure 1. A sieve analysis was performed to determine the particle size distribution and the same is referred in Table 1. Powder mix corresponding to Al-20% SiC was blended on a pot mill to obtain a homogeneous powder blend. The size of Silicon carbide powder mixed was 50, 65 and 120 micrometers. Green compacts of the powder blend was prepared on a 1.0 MN capacity hydraulic press using suitable punch and die assembly as shown in Figure 2. The compacting pressure applied was 517.566 MPa, which was maintained for all composition of SiC composites.

The free surfaces of the compacts were coated with an indigenously developed ceramic mixture [13] and dried under room-temperature conditions for a period of 9 hours. A second coating was applied at a direction of 90° to the direction of first coating and was allowed to dry for a further period of 9 hours under the same conditions as stated above.

2.2 Sintering

Sintering of powder sequentially involves the establishment and growth of bonds between the particles of powder at their areas of contact and migration of the grain boundaries formed at the bonds. Bonds form between the particles during sintering, and the number of particle bonds increases as the temperature increases.

X-ray diffraction (XRD) patterns of the specimen reinforced with 10 wt% SiC is shown in Figure 3. Al peaks and SiC peaks were indexed using JCPDS files (file number 040787 and

49-1431 respectively). The XRD pattern confirmed the presence of Al matrix and SiC particulate in the composite.

Table I: Characteristics of aluminium.

	Sieve number (μm)	**wt.% retained**
Aluminium	+106	00.26
	+90	02.54
	+75	14.73
	+63	17.58
	+53	24.86
	+45	12.33
	+38	06.27
	-38	21.42
Apparent density (g. cm^{-3})		1.030
Flow rate, (by Hall flow meter) (50 g^{-1})		32.00

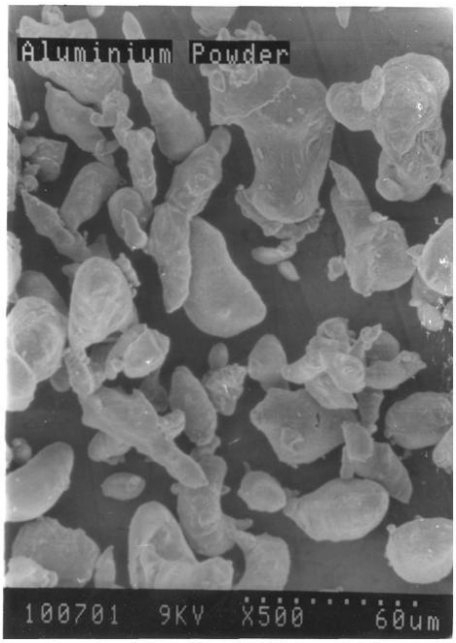

Figure 1: The SEM photograph of aluminium powder.

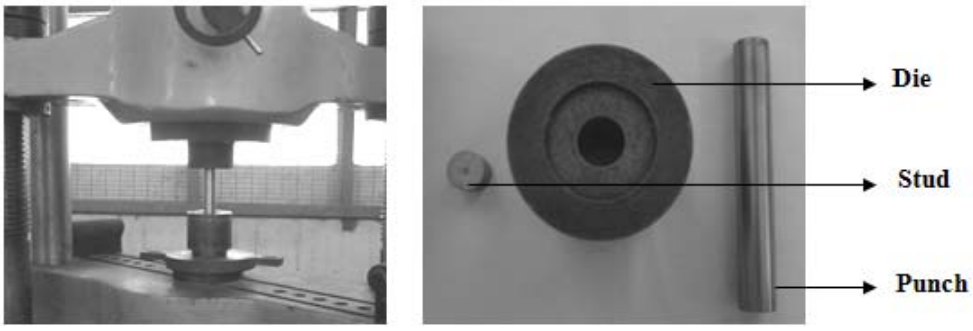

Hydraulic press Die set parts

Figure 2: Photographs of hydraulic press and parts of compacting Die.

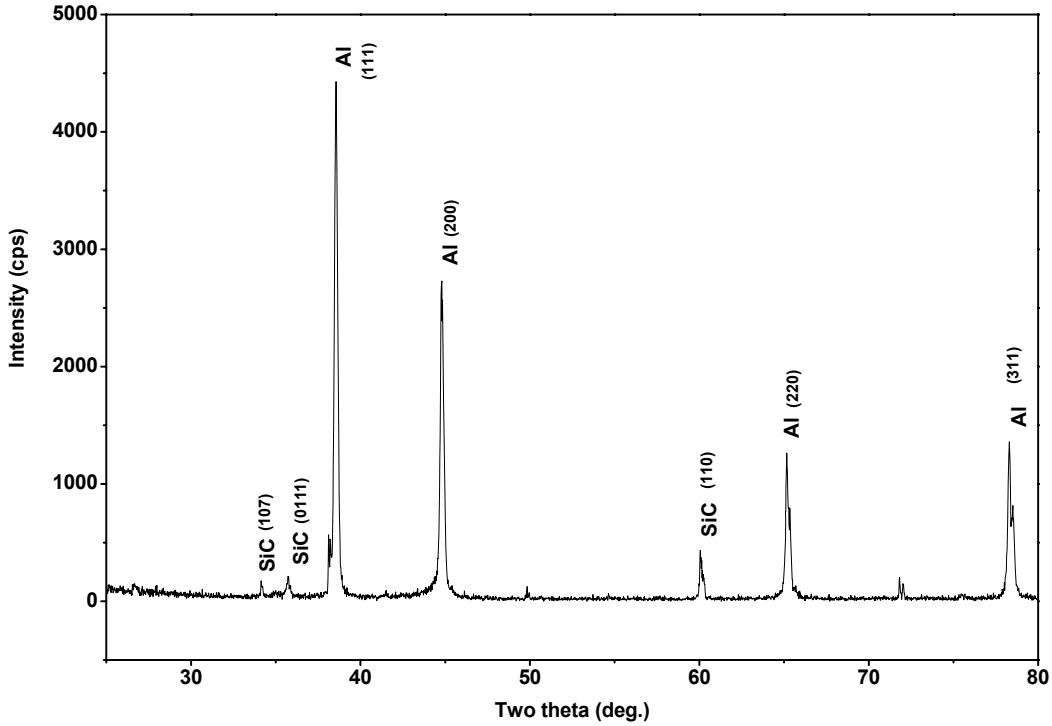

Figure 3: XRD results for the preform of Al-10% SiC composite.

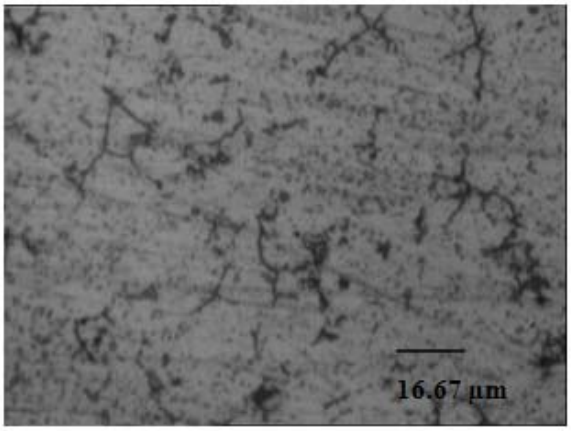

Figure 4(a): Microstructure of as sintered Al-0% SiC P/M perform.

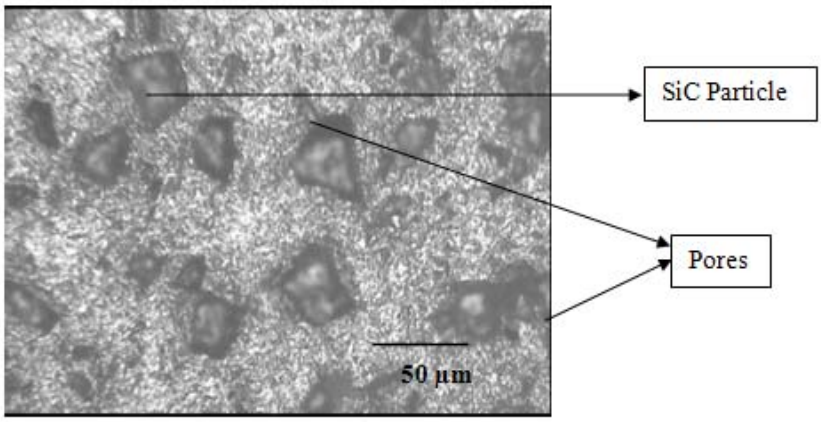

Figure 4(b): Microstructure of as sintered Al-20% SiC P/M perform – 50 microns.

Figures 4(a)-(d) show microphotographs of sintered preforms of Al with various particle sizes of SiC. In the case of sintering apart from bonding, the main factor affecting the properties of a sintered Al part is the amount of combined SiC formed in the Al. The maximum combined SiC content is achieved at 605°C, while additional strengthening at higher temperature is caused by increased sintering as is evident by the elimination of grain boundaries and spheroidization of pores. Time of sintering also affects the amount of combined SiC formed. The sintering time above 120 minutes leads to almost complete absence of grain boundaries and substantial spheroidization of pores. Accounting the aforementioned characteristics of sintered powder metallurgy Al-SiC, the ceramic-coated compacts were sintered in an electric muffle furnace in the temperature range of (605 ± 10)°C for a sintering time of 120 minutes and allowed to get cooled to room temperature in the furnace itself. The microstructure of sintered Al and 50 μm SiC added Al is shown as black color pores and white Al regions in Figures 4(a)-(b). Addition of 65 and 120 μm of SiC has resulted in reduced pores and more amount of Al with white background are shown in Figures 4(c)-(d). The ceramic coatings over the specimen were machined off and further machining was carried out to such dimensions, so that to obtain preforms with initial aspect ratios 0.9 and 1.2.

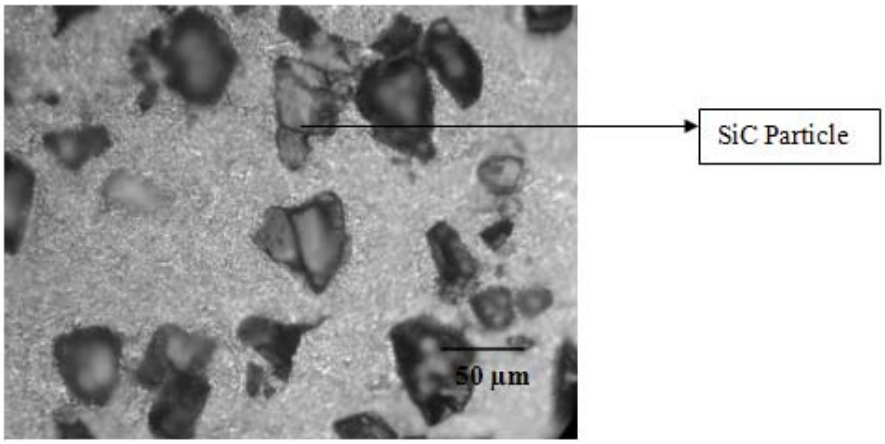

Figure 4(c): Microstructure of as sintered Al-20% SiC P/M perform – 65 Microns.

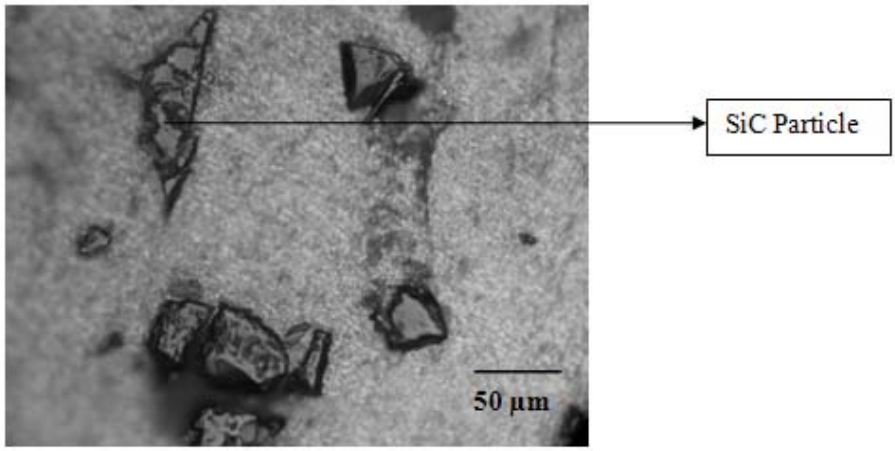

Figure 4(d): Microstructure of as sintered Al-20% SiC P/M perform – 120 Microns.

2.3 Deformation test

Initial diameter (D_0), initial height (h_0) and the initial preform relative density (ρ_0) of the specimen were measured and recorded. Each compact was subjected to the incremental compressive loads of 0.01 MN and the upsetting was carried between two flat, mirror finished

open dies on a hydraulic press of 1.0 MN capacity. The deformation was carried out until the appearance of first visible crack on the free surface. After each interval of loading, dimensional changes in the specimen such as height after deformation (h_f), top contact diameter (D_{TC}), bottom contact diameter (D_{BC}), bulged diameter (D_B) and density of the preform (ρ_f) were measured. The schematic diagram showing the various parameters measured before and after deformation is provided in Figure 5.

Using the Archimedes principle, the density of upset preforms was also determined after every loading interval. The deformation tests are continued until the fracture occurs at outer surface of the specimen as shown in Figure 6.

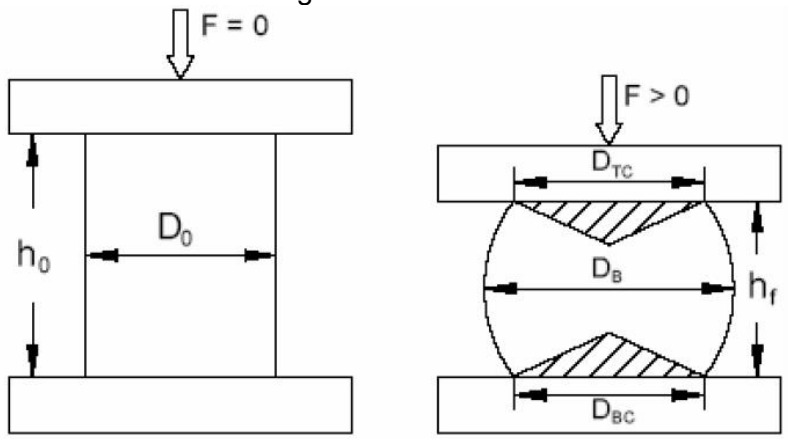

Figure 5: Upset test preform before and after deformation.

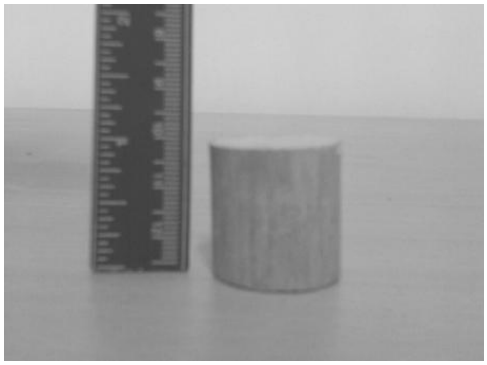

Before deformation

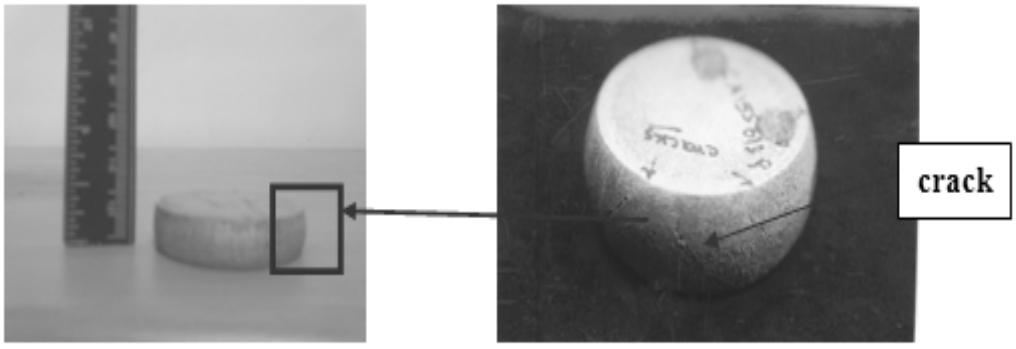

After Deformation

Figure 6: Photographs showing preform of before and after deformation test.

3. THEORETICAL INVESTIGATIONS

The various upsetting parameters under triaxial stress state condition are determined with the application of the following expressions.

3.1 Stress

The state of stress in a triaxial stress condition is given by Narayanasamy et al., [17] as follows:

$$\alpha = \frac{(2+R^2)\sigma_\theta - R^2(\sigma_Z + 2\sigma_\theta)}{(2+R^2)\sigma_Z - R^2(\sigma_Z + 2\sigma_\theta)} \quad (1)$$

From the Equation (1) for the known values of Poisson ratio (α), Relative density (R) and true axial stress (σ_z), the true hoop stress component (σ_θ) can be determined as follows:

$$\sigma_\theta = \left(\frac{2\alpha + R^2}{2 - R^2 + 2R^2\alpha}\right)\sigma_Z \quad (2)$$

At triaxial stress state condition, the relative density (R) of the compacts plays a vital role in the determination of the true hoop stress component (σ_θ).
The true hydrostatic stress is given by,

$$\sigma_m = \left(\frac{\sigma_r + \sigma_\theta + \sigma_z}{3}\right) \quad (3)$$

Since $\sigma_r = \sigma_\theta$ in the case of axisymmetric triaxial stress condition, the above equation becomes as follows:

$$\sigma_m = \left(\frac{\sigma_Z + 2\sigma_\theta}{3}\right) \quad (4)$$

The true effective stress can be determined from the following expression in terms of cylindrical coordinates as explained elsewhere [17]

$$\sigma_{eff}^2 = \frac{\sigma_z^2 + \sigma_\theta^2 + \sigma_r^2 - R^2\left(\sigma_z\sigma_\theta + \sigma_\theta\sigma_r + \sigma_z\sigma_r\right)}{\left(2R^2 - 1\right)} \quad (5)$$

Since $\sigma_r = \sigma_\theta$ for cylindrical axisymmetric upsetting operation, the true effective stress is determined as follows:

$$\sigma_{eff}^2 = \frac{\sigma_z^2 + 2\sigma_\theta^2 - R^2\left(\sigma_z\sigma_\theta + \sigma_\theta^2 + \sigma_z\sigma_\theta\right)}{\left(2R^2 - 1\right)} \quad (6)$$

The Equation 6 can be rewritten as

$$\sigma_{eff} = \left(\frac{\sigma_z^2 + 2\sigma_\theta^2 - R^2\left(\sigma_z\sigma_\theta + \sigma_\theta^2 + \sigma_z\sigma_\theta\right)}{\left(2R^2 - 1\right)}\right)^{1/2} \quad (7)$$

3.2 Formability stress index

As an evidence of experimental investigation implying the importance of the spherical component of the stress state on fracture, a parameter called a Formability Stress Index 'β' is given by,

$$\beta = \frac{3\sigma_m}{\sigma_{eff}} \tag{8}$$

This index determines the fracture limit as explained in the reference [9].

3.3 Strain

The true axial strain (ε_z) is expressed as given below:

$$\varepsilon_Z = \ln\left(\frac{h_0}{h_f}\right) \tag{9}$$

The true hoop strain (ε_θ) can be determined by the following expression as described elsewhere [17].

$$\varepsilon_\theta = \ln\left(\frac{2D_b^2 + D_c^2}{3D_o^2}\right) \tag{10}$$

The stress formability index (β) provided in the Equation 7 can be derived for the triaxial stress state condition.

4. RESULTS AND DISCUSSIONS

Figures 7 (a)-(b) have been plotted between various triaxial stresses namely the true hoop stress (σ_θ), the true effective stress (σ_{eff}) and the true mean stress (σ_m) and the true axial strain (ε_z) for Al containing three different SiC particle sizes namely 50, 65 and 120 μm and for two aspect ratios. For any given composition of composite, as the particle size of SiC increases, the true hoop stress (σ_θ), the true effective stress (σ_{eff}) and the true mean stress (σ_m) decreases. From these figures it is understood that the true hoop stress (σ_θ), the true effective stress (σ_{eff}) and the true mean stress (σ_m) are affected by the aspect ratios and its particle size. As a SiC particle size decreases the porosity level decreases and the relative density increases for the same compacting pressure. This may be one of the reasons for the increasing stresses for lower particle sizes of SiC added composite.

Figure 8 has been plotted between the formability stress index (β) and the relative density for Al containing three different SiC particle sizes and for two different aspect ratios namely 0.9 and 1.2. The slope value between the formability index (β) and the relative density increase with increasing of SiC content. The SiC particle occupies the pores between Al particles. Since the pore size is very small, formability stress index value increases during plastic deformation. Pure Al makes bigger pores, and hence the formability index (β) value also reduces. It is further observed that the pore size becomes smaller and smaller for the lower sizes of SiC content and hence the formability stress index value also increases. As the aspect ratio increases the formability stress index decreases because of more porous bed height. This indicates that the aspect ratio value 0.9 (smaller value) shows better densification compared to other aspect ratio.

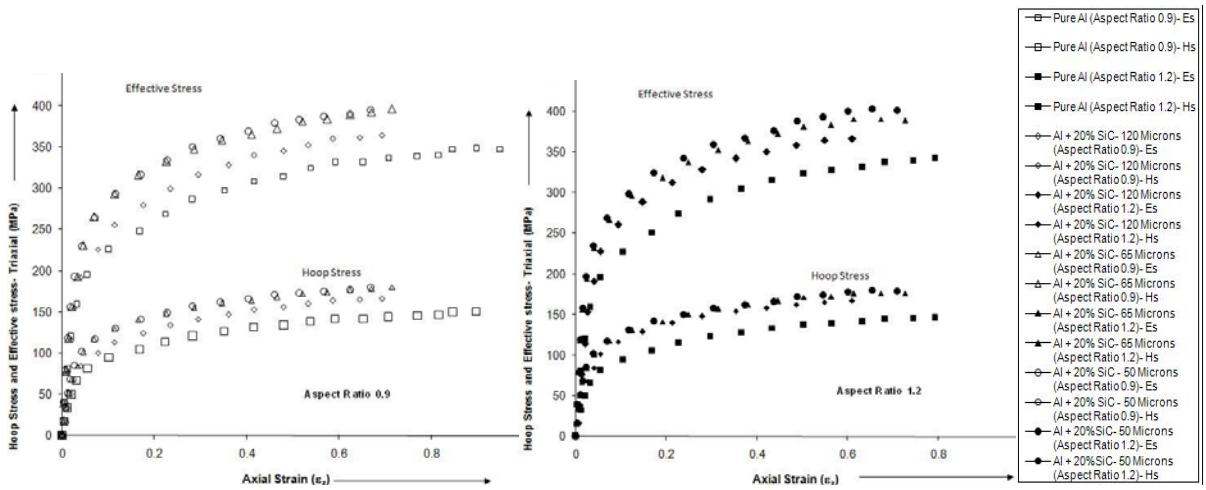

Figure 7(a): The variation of true Hoop stress (σ_θ) and true effective stress (σ_{eff}) with respect to the True Axial strain (ε_z) under triaxial stress state condition.

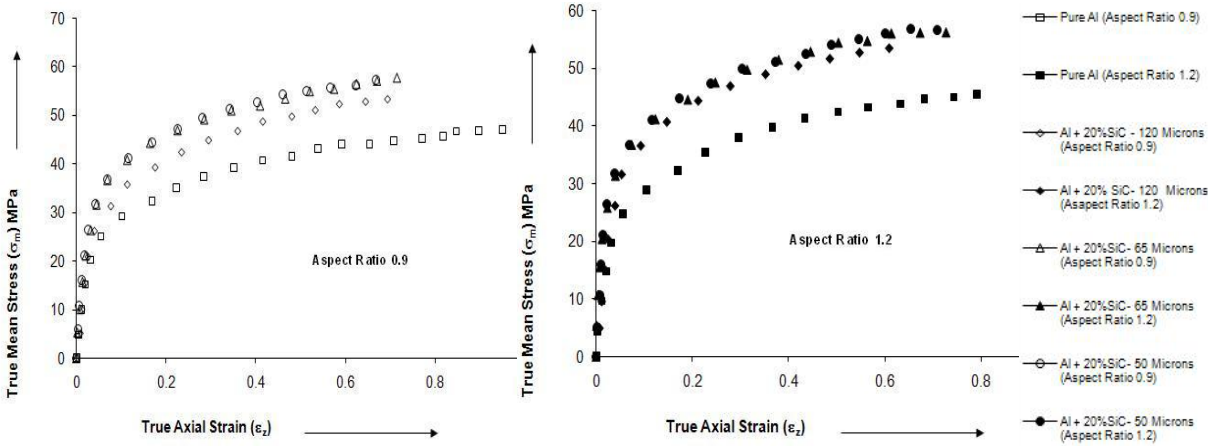

Figure 7(b): The variation of true mean or hydrostatic stress (σ_m) with respect to the true axial strain (ε_z) under triaxial stress state condition.

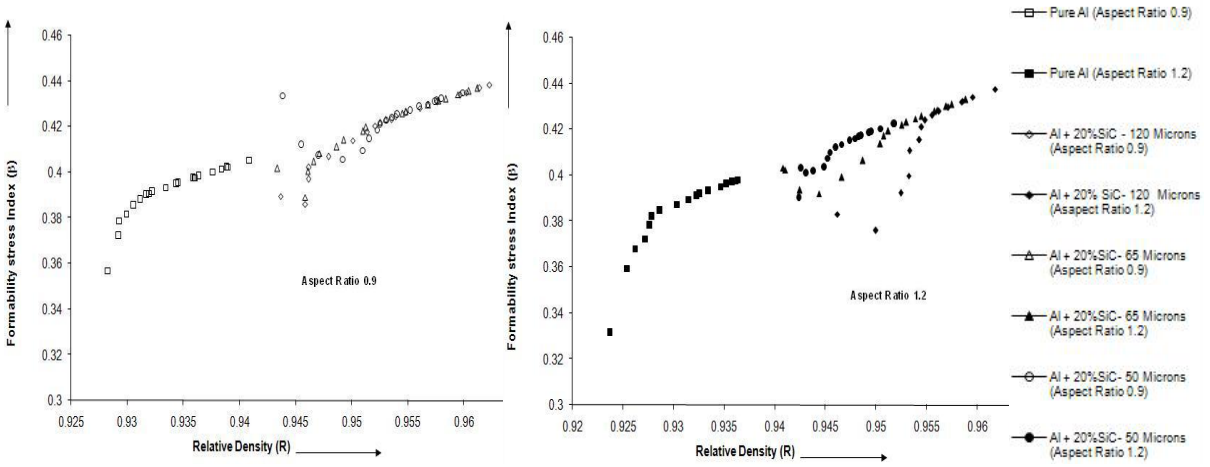

Figure 8: The variation of formability stress index (β) with respect to the relative density (R) for Al-20% SiC composite.

Figure 9 has been plotted between the stress ratio parameter ($\sigma_\theta / \sigma_{eff}$) and the Relative density (R) for Al containing three different SiC particle sizes and for two different aspect ratios namely 0.9 and 1.2. As the Relative density increases, the stress ratio parameter ($\sigma_\theta / \sigma_{eff}$) also increases because the true hoop stress (σ_θ) continues to increase rapidly during deformation. As the SiC particle size increases the stress ratio parameter ($\sigma_\theta / \sigma_{eff}$) is found to be higher compared to pure Al. In the case of pure Al the pore size is larger compared to Al-SiC composites and these results in lower stress ratio parameter ($\sigma_\theta / \sigma_{eff}$) value. The stress ratio parameter decreases with an increasing aspect ratio.

Figure 10 has been plotted between the stress ratio parameter (σ_z / σ_m) and the relative density (R) for Aluminium containing three different SiC particle sizes and for two different aspect ratios namely 0.9 and 1.2. As the SiC particle size increases, the stress ratio parameter decreases because Al-SiC composite exhibits fine pores compared to pure Al. In the case of fine pores, higher SiC particle size added composite increases the true mean stress (σ_m) value required for deformation and therefore the stress ratio parameter (σ_z / σ_m) decreases with increase in SiC particle size. As the aspect ratio increases to 1.2, the true mean stress (σ_m) value further increases and the true strain required for plastic deformation also increases before fracture. Here it is possible to conclude that the true mean stress (σ_m) value is well associated with the pore size.

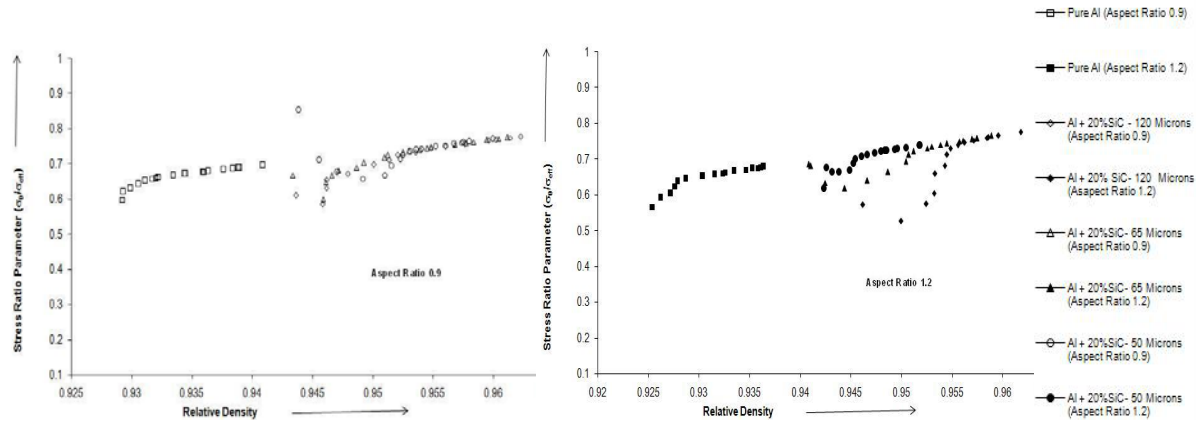

Figure 9: The variation of stress ratio parameter ($\sigma_\theta/\sigma_{eff}$) with respect to the relative density (R) for Al-20% SiC composite.

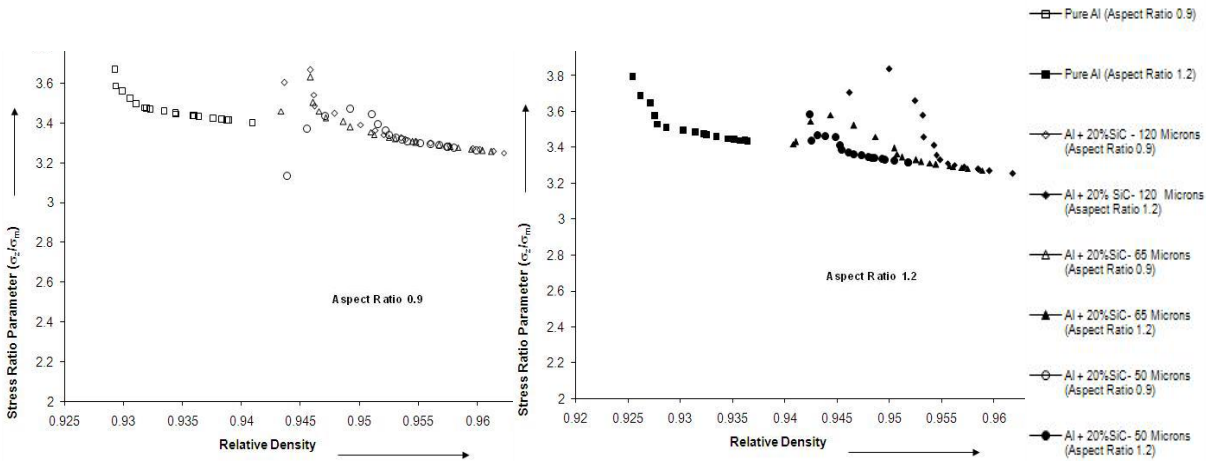

Figure 10: The variation of stress ratio parameter (σ_z / σ_m) with respect to the relative density (R) for Al-20% SiC composite.

Figures 11 (a)-(b) have been plotted between the fracture strain (ε_f) and the formability stress index (β) for the upsetting of Al, Al–SiC powder compacts of three different particle size

addition of SiC and for two different aspect ratios under triaxial stress state condition. It is observed that the fracture strain of the preform depends on the percentage addition of SiC. From this figure, it is further noted that for preforms with higher particle size of the SiC, the initiation of crack appears at a lower fracture strain value. However, it exhibited higher formability stress index (β). As the aspect ratio increases to 1.2, the fracture strain (ε_f) and the formability stress index (β) value decreases.

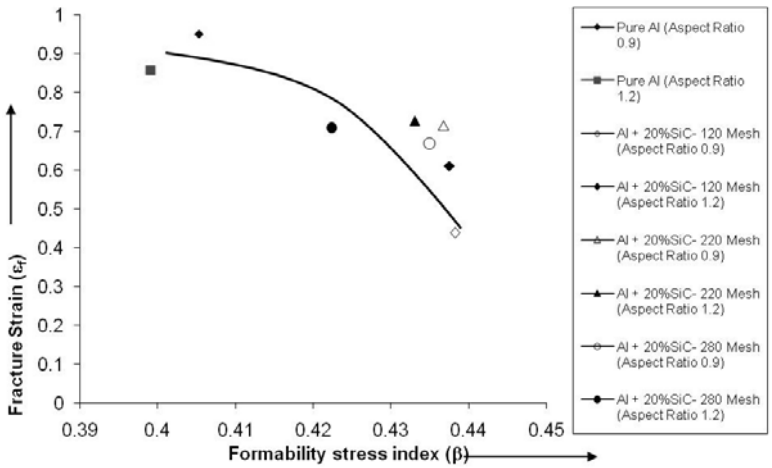

Figure 11: The variation of fracture strain (ε_f) with respect to formability stress Index (β).

5. CONCLUSIONS

The following conclusions can be drawn from the above results and discussions.

- As the Silicon carbide particle size increases the pore size becomes smaller.
- As the pore size becomes smaller, the formability stress value increases.
- Aspect ratio 0.9 shows higher formability stress value compared to aspect ratio 1.2 because of better densification.
- The stress ratio parameters ($\sigma_\theta / \sigma_{eff}$) is found to be higher for Al-SiC composites compared to pure Aluminium because of better densification.
- The stress ratio parameters (σ_z / σ_m) decreases in the case of Al-SiC composites compared to pure Aluminium because of fine pore size associated with high hydrostatic stress (σ_m).
- For preforms with higher particle size addition of SiC, the initiation of crack exhibits at lower fracture strain.
- For the higher aspect ratio, the relative density decreases.

NOMENCLATURE

F	Force applied on the cylindrical preform for deformation
h_0	Initial height of the cylindrical preform
h_f	Height of the barreled cylinder after deformation
D_0	Initial diameter of the preform
D_B	Bulged diameter of the preform after deformation
D_{TC}	Top contact diameter of the preform after deformation
D_{BC}	Bottom contact diameter of the preform after deformation
α	Poisson's ratio
σ_z	True stress in the axial direction
σ_θ	True stress in the hoop direction
σ_r	True stress in the radial direction

σ_{eff} Effective stress
σ_m Hydrostatic stress
σ True stress
ε True strain
ε_z True strain in the axial direction
ε_θ True strain in the hoop direction
ε_r True strain in the radial direction
β Formability Stress Index
ρ_o Initial preform density of the preform
ρ_f Density of the preform after deformation
ρ_{th} Theoretical density of the fully dense material
$R(or)\frac{\rho_f}{\rho_{th}}$ Relative density

REFERENCES

[1] Yulong Li , K.T. Ramesh, E.S.C. Chin, (2004). The mechanical response of an A359/SiCp MMC and the A359 aluminum matrix to dynamic shearing deformations, Material Science and Engineering A, Vol. 382, 162–170.

[2] Yulong Li , K.T. Ramesh, E.S.C. Chin, (2004). Comparison of the plastic deformation and failure of A359/SiC and 6061-T6/Al2O3 metal matrix composites under dynamic tension, Material Science and Engineering A, Vol. 371, 359–370.

[3] Y.X. Lu, X.M. Meng, C.S. Lee, R.K.Y. Li, C.G. Huang, J.K.L. Lai, (1999). Microstructure and mechanical behaviour of a sic particles Reinforced Al-5cu composite under dynamic loading, Journal of materials processing technology, Vol. 94, 175-178.

[4] Ze wen huang, Ian R. Mccoll, Samuel J. Harris, (1996). Notched behaviour of a silicon carbide particulate reinforced Aluminium alloy matrix composite, Materials science and engineering A Vol. 215, 67-72

[5] S.Szczepanik, W. Lohnert, (1996). The formability of the Ai-5%SiC composite obtained using p/m method, Journal of materials processing technology, Vol. 60, 703-709

[6] Edited by George.E. Dieter, ASM publications, USA, 2000, Hand book on workability analysis and applications.

[7] Shima, S., Oyane, M, (1976). Plasticity theory for porous metals, International Journal of Mechanical Sciences, Vol. 18, 285–291.

[8] Doraivelu, S.M., Gegel, H.L., Gunasekaran, J.S., Malas, J.C., Morugan, J.T., (1984). A new yield function for compressible P/M materials, International Journal of Mechanical Sciences, Vol. 26,No. (9/10), 527–535.

[9] M.Abdel-Rahman, M.N.El-Sheikh, (1995). Workability in forging of powder metallurgy compacts, Journal of materials processing technology, Vol. 54, 97-102.

[10] R. Narayanasamy, R. Ponalagusamy, (2000) A mathematical theory of plasticity for the upsetting of compressible P/M materials, Journal of materials processing technology, Vol. 97, 107-109.

[11] P.S.Satsangi, P.C.Sharma, R.Prakash, (2003) An elastic-plastic finite element method for the analysis of powder metal forging, Journal of materials processing technology, Vol. 136, 80-87.

[12] R. Narayanasamy, R. Ponalagusamy, K.R. Subramanian, (2001) Generalised yield criteria of porous sintered powder metallurgy metals, Journal of materials processing technology, Vol. 110, 182-185.

[13] R. Narayanasamy, T. Ramesh, K.S. Pandey, (2005). Some aspects on workability of aluminium–iron powder metallurgy composite during cold upsetting, Material Science and Engineering A, Vol. 391, 418–426.

[14] ASM International; 2002, Production Sintering Practices. In: Powder Metal Technologies and Applications, ASM Handbook, Vol.07, pp. 468- 503.

[15] R. Narayanasamy, T. Ramesh, K.S. Pandey, S.K. Pandey, (2008). Effect of particle size on new constitutive relationship of aluminium–iron powder metallurgy composite during cold upsetting, Matererials and Design, Vol. 29, 1011–1026.